Cantilever magnetoelectric PZT/Tb–Fe–Co resonators for magnetic sensing applications

N. Ngoc, G. Agnus, S. Matzen, T. Maroutian, D. Giang, P. Lecoeur

APL Materials

Cantilever magnetoelectric PZT/Tb–Fe–Co resonators for magnetic sensing applications

Cite as: APL Mater. 9, 041103 (2021); https://doi.org/10.1063/5.0042379
Submitted: 30 December 2020 . Accepted: 17 March 2021 . Published Online: 01 April 2021

N. T. Ngoc, G. Agnus, S. Matzen, T. Maroutian, D. T. Huong Giang, and P. Lecoeur

Cantilever magnetoelectric PZT/Tb–Fe–Co resonators for magnetic sensing applications

Cite as: APL Mater. 9, 041103 (2021); doi: 10.1063/5.0042379
Submitted: 30 December 2020 • Accepted: 17 March 2021 •
Published Online: 1 April 2021

N. T. Ngoc,[1,2] G. Agnus,[1,a)] S. Matzen,[1] T. Maroutian,[1] D. T. Huong Giang,[3] and P. Lecoeur[1]

AFFILIATIONS

[1] Université Paris-Saclay, CNRS, Centre de Nanosciences et de Nanotechnologies, 91120 Palaiseau, France
[2] Department of Advanced Materials Science and Nanotechnology, University of Science and Technology of Hanoi, Vietnam Academy of Science and Technology, 18 Hoang Quoc Viet, Hanoi, Vietnam
[3] University of Engineering and Technology, Vietnam National University, Hanoi, Vietnam

Note: This paper is part of the Special Topic on Magnetoelectric Materials, Phenomena, and Devices.
[a)] **Author to whom correspondence should be addressed:** guillaume.agnus@universite-paris-saclay.fr

ABSTRACT

Magnetoelectric material-based cantilever resonators have been considered as a promising solution for magnetic sensing applications. However, most applications focus on bulk piezoelectric (e.g., PZT) laminated composites, which put a critical limit for miniaturizing into micrometer-sized devices. This work aims at demonstrating the potential of a micro-resonator approach with lower power consumption and smaller size. It reports on the fabrication and characterization of a resonant cantilever based on a freestanding multi-ferroic PZT/Tb–Fe–Co thin film multilayer, where the magnetic signal is sensed by measuring the shift of the device resonant frequency. The Tb–Fe–Co layer acts as a magnetic field sensing layer, while the PZT thin film integrated in the capacitor geometry acts as a micro-transducer to obtain an electrical signal. For a magnetic field less than 0.2 T, a sensitivity as high as 487 Hz/T is measured for the sensor under a vacuum environment. While the sensor design has to be further optimized to improve the performance, it is promising as a micro-magnetoelectric sensor for magnetic field sensing.

INTRODUCTION

Magnetoelectric (ME) sensors convert directly a magnetic signal into an electrical one through the mechanical coupling between a ferromagnetic material and a piezoelectric (PZT) one in a multiferroic laminated composite.[1–3] The sensitivity of ME resonators with a low magnetic noise floor of about $\mathrm{pT}/\sqrt{\mathrm{Hz}}$ at 1 Hz[4–6] is remarkably high compared to other different magnetometers. This allows us to imagine new devices based on coupled layers for magnetic sensing applications for a high signal to noise ratio. Up to now, the studies of bulk magneto-electrostrictive composites, composed by a piezoelectric and a magnetostrictive laminate, achieved remarkable success with magnetoelectric coefficients up to 21.6 V/cm Oe[2,3,7,8] (corresponding to 27.12 V/A). However, targeting to microscale applications to provide lower power consumption and higher integration, miniaturization is necessary. It requires being able to grow the full hetero-structure on top of silicon substrates in order to take advantage of the conventional clean room processes for the realization of the microsystem. The growth of epitaxial thin films of piezoelectric materials on top of silicon has been demonstrated by using Pulsed Laser deposition (PLD), with good electromechanical properties of piezoelectric layers.[9,10] For the fabrication of a ME micro-sensor, the growth of the two functional layers (magnetostrictive and piezoelectric) directly on top of each other in close contact is expected to enhance the mechanical coupling and to avoid any interfacial layer such as glue that limits the stress transfer. In addition, the use of the self-excitation capability of piezoelectric materials, such as in resonance-based biosensors or mass detectors whose general working principle is based on the frequency shift of devices due to stress from external factors,[11,12] allows us to avoid the need for solenoid coils in microdesign compared to the conventional ME sensors using AC magnetic field drives. Currently, ME micro-resonators in the form of cantilevers have thus attracted significant attention due to larger mechanical strains in the ferroelectric

phase, leading to higher output response.[5,13] The working principle of such resonators is straightforward: The stress induced in the magnetic layer under external magnetic fields is transmitted to the piezoelectric layer, resulting in a change in the resonant frequency of the system. This shift of the resonant frequency can be detected by impedance measurement. The sensitivity of sensors can be defined as the ratio of the change in the resonant frequency to the range of the external DC magnetic field ($sensitivity = df/dB$).[13,14]

Bennett *et al.*[13] reported for doubly clamped magnetoelectric micro-electromechanical-systems (MEMSs) of AlN (750 nm)–FeCo (200 nm) resonators a magnetic field sensitivity of about 5000 Hz/T in a bias magnetic field of up to 0.2 T. In this work, we will demonstrate the potential of a full PZT/Tb–Fe–Co thin film heterostructure as a resonator in the form of a cantilever with one free end (single clamped MEMS) for magnetic sensing applications.

MICROFABRICATION AND EXPERIMENTAL METHODS

The heterostructure used in this work (see Fig. 1) consists of a magnetostrictive $Tb(Fe_{0.55}Co_{0.45})_{1.5}$ (Tb–Fe–Co) layer, which also serves as the top electrode; a piezoelectric $PbZr_{0.52}Ti_{0.48}O_3$ (PZT) layer; and a $SrRuO_3$ (SRO) bottom electrode. A double buffer layer of Yttria-Stabilized Zirconia or YSZ (8 mol. $\%Y_2O_3$-doped ZrO_2) (90 nm)/CeO_2 (20 nm) is used to consume (with YSZ) the native SiO_2 layer at the surface of the silicon (001) substrate before the following epitaxial layers and to lower (with CeO_2) the lattice mismatch between YSZ (lattice parameter of 0.541 nm) and perovskite oxide layers.[15,16] All layers are grown by Pulsed Laser Deposition (PLD) with a KrF excimer laser at 248 nm wavelength, a laser-repetition rate of 4 Hz, and an energy density of 2.7 J/cm^2. YSZ and CeO_2 were deposited at 750 °C in 2×10^{-4} Torr oxygen, with a dedicated two-step growth process for YSZ on silicon.[16] A 40 nm-thick SRO film was epitaxially grown at 640 °C in 0.12 Torr oxygen on the YSZ/CeO_2 buffer layer. A PZT piezoelectric film with a thickness of 150 nm was deposited with 0.12 Torr nitrous oxide (N_2O) and at a substrate temperature of 640 °C [Fig. 1(b)]. A multi-step process (detailed in Fig. 1) was used to define cantilevers of 40 μm length and 20 μm width. The microfabrication process begins with an etching step down to the silicon substrate to structure the desired shape of cantilevers using lithography and Ion Beam Etching (IBE) methods [Fig. 1(c)]. In order to protect the desired area, a thick TI35ES photoresist was used, which gives a 4 μm-thick layer with a spinning speed of 4000 rotation per minute (RPM). Ar ions were used to sputter the sample during the IBE process.

In order to ensure the electrical contact to the bottom electrode, a window is opened by etching down to the SRO layer using IBE and a 100 nm-thick platinum (Pt) electrode is deposited on the SRO layer [Fig. 1(d)] through a lift-off process. The magnetostrictive thin film Tb–Fe–Co is deposited by radio frequency (RF) magnetron sputtering with an applied power of 75 W and Ar pressure of 2.2 mTorr [Fig. 1(e)] using a lift-off process. The distance between the sample and the target is fixed at 5 cm. After depositing the Pt electrode on top of the Tb–Fe–Co layer [Fig. 1(f)], the cantilever magnetoelectric PZT/Tb–Fe–Co resonators have been released from the Si substrate by sacrificial etching of the underlying silicon structure using XeF_2 isotropic etching [Fig. 1(g)]. Finally, the bottom and top contacts were electrically connected using wire bonding [Fig. 1(h)].

The crystalline quality of the fabricated PZT thin films was determined by x-ray diffraction (XRD) with a PANalytical X'Pert Pro diffractometer. The x-ray source is a Cu based one with a Ge (220) four-crystal monochromator. In order to evaluate the ferroelectric properties, the dielectric constant (ε) of the PZT thin

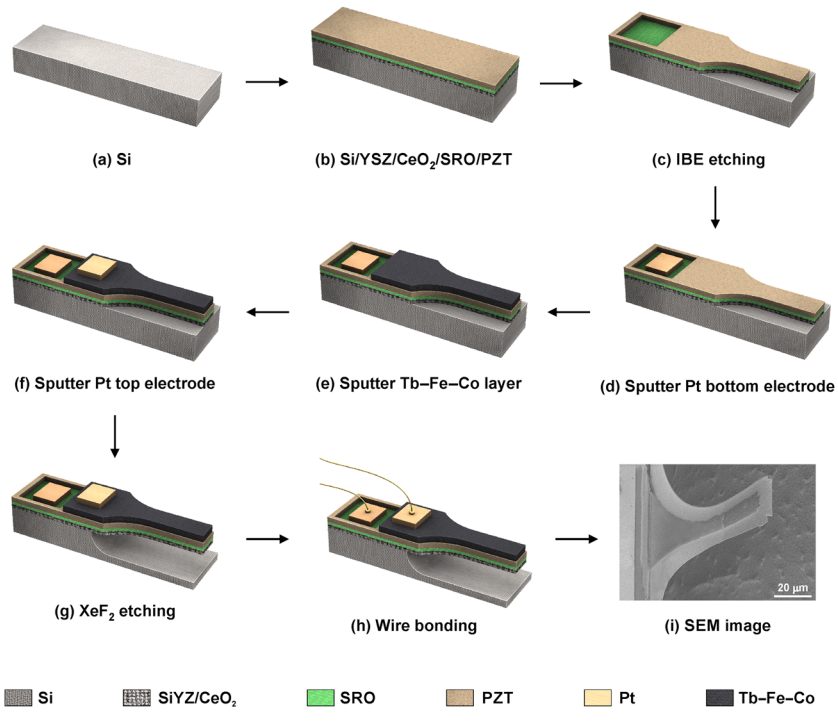

FIG. 1. (a)–(h) The schematics of the patterning steps for the fabrication of magnetoelectric PZT/Tb–Fe–Co micro-resonators. (i) Scanning electron microscopy image of the fabricated cantilever that has a length of 40 μm and a width of 20 μm.

film was extracted from capacitance–voltage (C–V) characteristics as defined by $\varepsilon = C \cdot t/(\varepsilon_0 \cdot A)$, where t is the thickness of the PZT layer, ε_0 is the permittivity of the free space, and A is the area of the top electrode. The static deformation of the PZT cantilever under an external DC electric field was observed using optical profilometry.[17]

The frequency response of the cantilever was measured with an impedance analyzer (Hioki IM3570) to verify the self-excitation capability of the fabricated piezoelectric cantilever. The application of the electric field on the PZT layer induces strain through the inverse piezoelectric effect. An exciting AC bias superimposed with a DC voltage at frequency around the resonance of the cantilever was carried out to characterize the frequency response of the PZT cantilever. Such a piezoelectric cantilever was then used as the core element in the ME sensor for magnetic field measurement. A Tb–Fe–Co thin film with a thickness of 150 nm was deposited on top of the PZT layer to create a ME device. Since previous studies on Tb–Fe–Co thin films[18,19] show that as-deposited films exhibit a perpendicular magnetic anisotropy, the device is measured under an external magnetic field perpendicular to the surface to characterize the frequency response of the ME Tb–Fe–Co/PZT device. The study of this ME based magnetic sensor is carried out at atmospheric pressure and at 0.5 mbar pressure to reduce air damping, as shown in Fig. 2. A dipole electromagnet was used for the homogeneous DC magnetic field up to 1 T, in which the positive direction of the field was defined from the bottom electrode to the top electrode of the samples.

RESULTS AND DISCUSSION

Figure 3 shows that the PZT film exhibits a (110)-oriented single-phase perovskite structure with only high intensity peaks of the (110) family, as is usually found for PZT films on SRO layers on the silicon substrate.[20] The full width at half maximum of about 1.94° of the rocking-curves of the (110) PZT diffraction peak shows a typical quality PZT thin film.[21]

Figure 4(a) shows the dielectric constant hysteresis curve of the PZT thin film. For the PZT thin film with a thickness of 150 nm, the coercive field (E_c) is about 60 kV/cm. The static deformation of the PZT cantilever characterized by the maximum deflection at the free end as a function of DC field up to close to 300 kV/cm was measured and plotted in Fig. 4(b), where the deflection of the cantilever

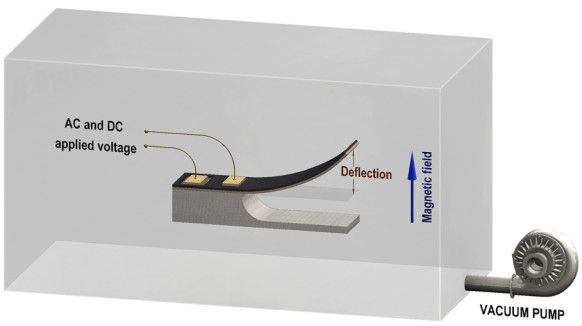

FIG. 2. The experimental setup for resonance characterization of the cantilever sample.

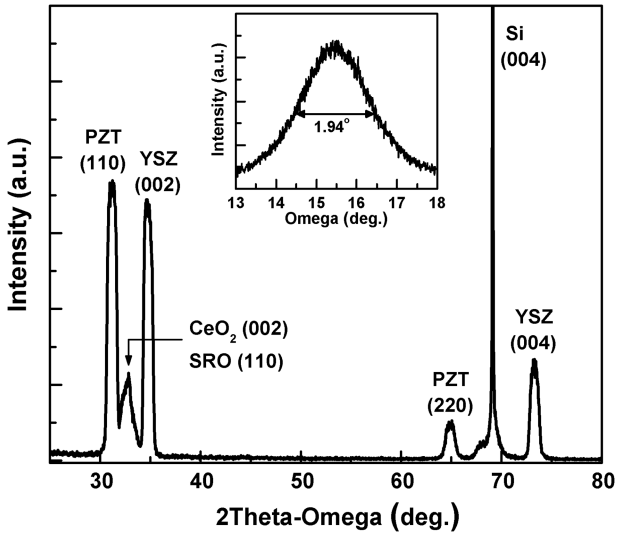

FIG. 3. The XRD patterns of PZT thin films on SRO/CeO_2/YSZ/Si(001) and (insert) corresponding ω-scan rocking curve of the PZT (110) peak.

is illustrated as shown in Fig. 2. As the cantilevers are composed of active (PZT layer) and inactive layers, when a DC electric field is applied to the PZT layer across the two electrodes, the strain gradient will change the shape of the PZT layer because of the inverse

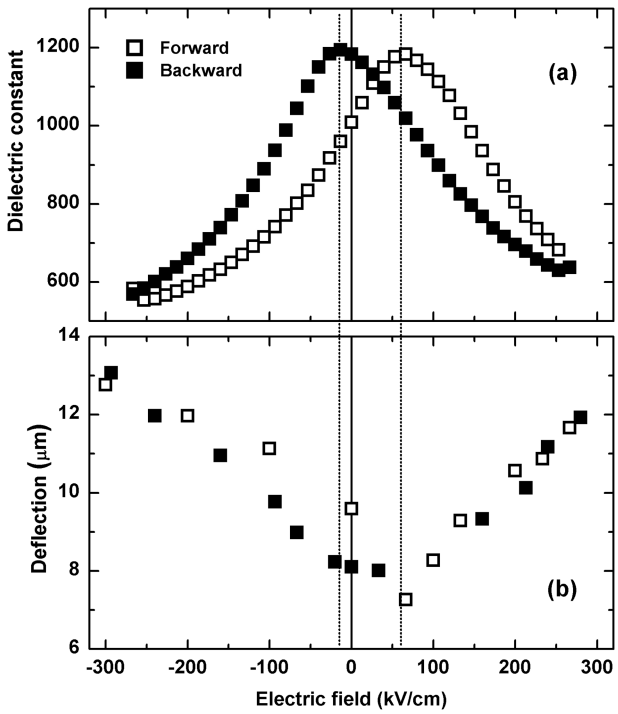

FIG. 4. (a) The dielectric constant hysteresis curve and (b) interferometric profilometry measurements of the PZT cantilever displacements collected at the free end.

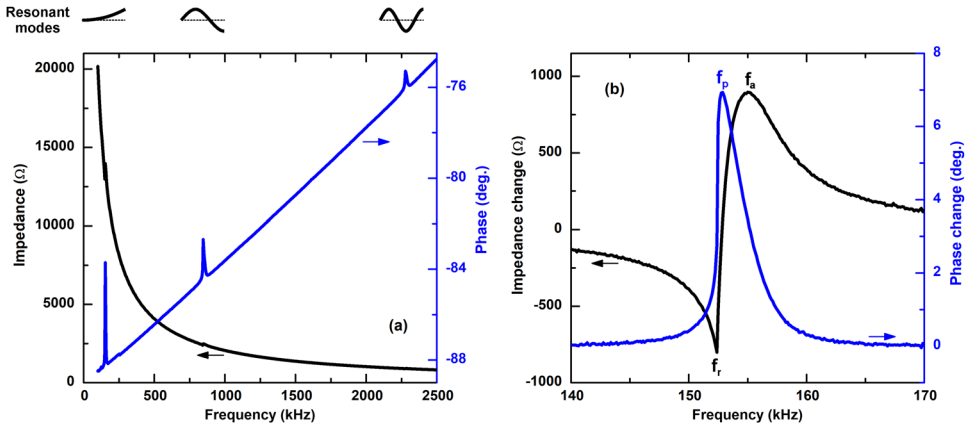

FIG. 5. (a) A changing impedance and phase were measured as a function of the frequency of the AC excitation (V_{AC} = 100 mVpp, V_{DC} = 0 in this case) sweeping in a large range to sense the first three modes of resonance. (b) The electrical signal shown in (a) for the first resonant mode with background subtracted.

piezoelectric effect, leading to the observed deformation of the cantilever due to boundary conditions at the inactive layers.

An upward bending of the cantilever of around 8 μm at the cantilever free end already exists even at zero DC bias voltage that is explained by the residual stress gradient in the cantilever even after the releasing step. The presence of residual stresses is unavoidable during the deposition of such a complex stack, which leads to the initial bending of the cantilever. The residual stress originates from the mismatch in the thermal expansion coefficients of the different deposited materials and from the lattice mismatch between each layer during the deposition. It is observed that the deflection curve follows the conventional butterfly shape of the C–E curve with a total variation of 6 μm. At a high electric field, the deflection of the cantilever is maximum, while it is minimum around the switching voltage (disordered polarization state of PZT). The observed maximum deflections are higher than the 2 μm displacement measured for a 2 μm-thick PZT cantilever at 20 V (corresponding to 200 kV/cm applied electric field), with sol-gel deposited PZT, by Ambika *et al.*[22] Using the procedure described by Weinberg,[23] a value of d_{31} of about -53 pm V^{-1} was estimated from the slope of the linear dependence of deflection with the electric field. This value is smaller than that of similar 1 μm-thick PZT films (-118.9 pm V^{-1}) reported by Dekkers *et al.*[24] By the same group, a d_{31} of -97 pm V^{-1} was reported on 750-nm-thick $Pb(Zr_{0.52}Ti_{0.48})O_3$.[9] This smaller value can be explained due to the use of a thinner PZT layer in our devices, as reported by Haccart *et al.*[25]

The self-excitation capability of the PZT cantilever prior to the deposition of the Tb–Fe–Co layer was shown in Fig. 5(a) where the first three resonant modes of the PZT cantilever at 154.40, 846.75, and 2278.60 kHz are shown. The frequency ratios between the modes 1:5.48:14.75 illustrate the corresponding modal shapes. These experimental ratios are in good agreement with the calculated result for typical cantilevers,[26] thus hinting that these are indeed the first three bending modes of the cantilever.

Due to the higher amplitude and higher stability of the output signal, the first resonant mode of vibration of the cantilever was generally chosen in order to investigate its electromechanical properties. Figure 5(b) shows a zoomed-in view of the frequency range of the first mode after subtracting the background signal. From the diagram, the resonance (f_r) and anti-resonance (f_a) peaks in the impedance spectra and a peak in the impedance phase angle (f_p) were measured to further evaluate the shifting resonance of the device.

Figure 6 shows the performance of the PZT cantilever as a resonator for sensing a shift of the resonant frequency f_r under the strain generated by the applied field. The resonant frequency was measured as a function of the DC bias applied to the PZT cantilever. In these measurements, an AC sine-wave of 200 mVpp in the frequency range from 140 to 175 kHz to measure the first mode of vibration was superimposed on a DC bias and applied to the top electrode while the bottom electrode was grounded. The DC bias was swept from −4 to 4 V (corresponding to −266 to 266 kV/cm)

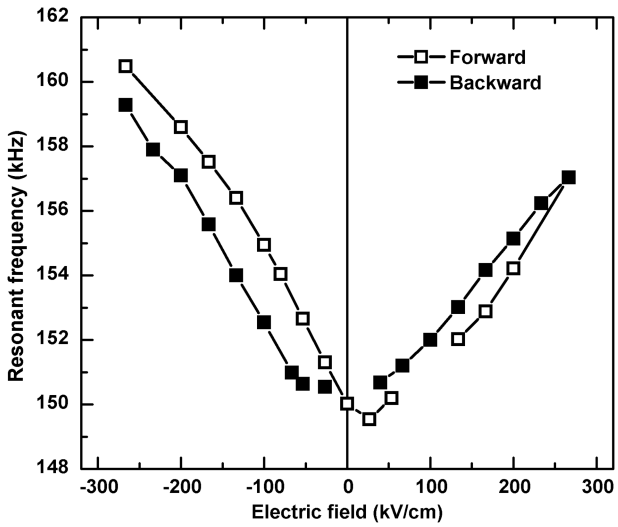

FIG. 6. The resonant frequency f_r as a function of the electric field obtained upon the application of a DC bias to the PZT thin film, from −266 to 266 kV/cm (forward) and from 266 to −266 kV/cm (backward).

and then back to −4 V. The shift of the resonant frequency plotted in Fig. 6 follows a butterfly shape, which is consistent with the deformation of the cantilever under the application of the electric field, as shown in Fig. 4(b). The missing points are due to negligible deflections of the cantilever measured around the PZT switching voltages.

A clear shift of the resonant frequency can thus be observed when the cantilever is stressed, allowing us to expect a signal from a sensor where the stress is generated by a magnetostrictive material.

A DC magnetic field was sensed by focusing on the change in the impedance phase angle frequency peak (f_p) of the magnetoelectric PZT/Tb–Fe–Co cantilever resonators. Figure 7(a) shows the curves of the impedance phase as a function of the frequency with the sweeping rate of 1200 Hz/min under two values of external DC magnetic fields at atmospheric pressure. The cantilever is excited by an AC bias of 100 mVpp superimposed on a DC voltage of −2.5 V (corresponding to −166 kV/cm) in a frequency range close to the resonant frequency. The electric field of −166 kV/cm is chosen due to the highest sensitivity of resonant frequency with respect to the electric field, as shown in Fig. 6. The results indicate that the resonance phenomenon occurs at different frequencies when changing the external magnetic field. The resonant frequency f_p extracted from the maximum value of the impedance phase peak as a function of the out-of-plane DC magnetic field at atmospheric pressure are shown in Fig. 7(b). The measurement as a function of magnetic field [Figs. 7(b) and 7(d)] was performed in "point-by-point" mode. The V-shape of the curves following the typical shape of the magnetoelastic properties of the magnetostrictive Tb–Fe–Co layer[27,28] demonstrates that the main contribution to the resonant frequency change is from the induced magnetostrictive strain. The magnetic field sensitivity is about 300 Hz/T under atmospheric pressure.

In order to evaluate the loss due to air damping, the sensor response was explored in a 0.5 mbar vacuum environment, as shown in Figs. 7(c) and 7(d). For measurement, the magnitude of the AC voltage has to be small enough to minimize nonlinear effects but also high enough to stimulate the cantilever's oscillation. Due to the reduction of air damping when working under vacuum, a smaller driving AC voltage was chosen under vacuum for the cantilever's excitation. An AC excitation of 10 mVpp superimposed with a DC voltage of −2.5 V (corresponding to −166 kV/cm) and an out-of-plane DC magnetic field were used. Figure 7(c) shows sharp resonant peaks, and these peaks occur at higher frequencies in vacuum compared to the case in atmospheric pressure. This can be explained due

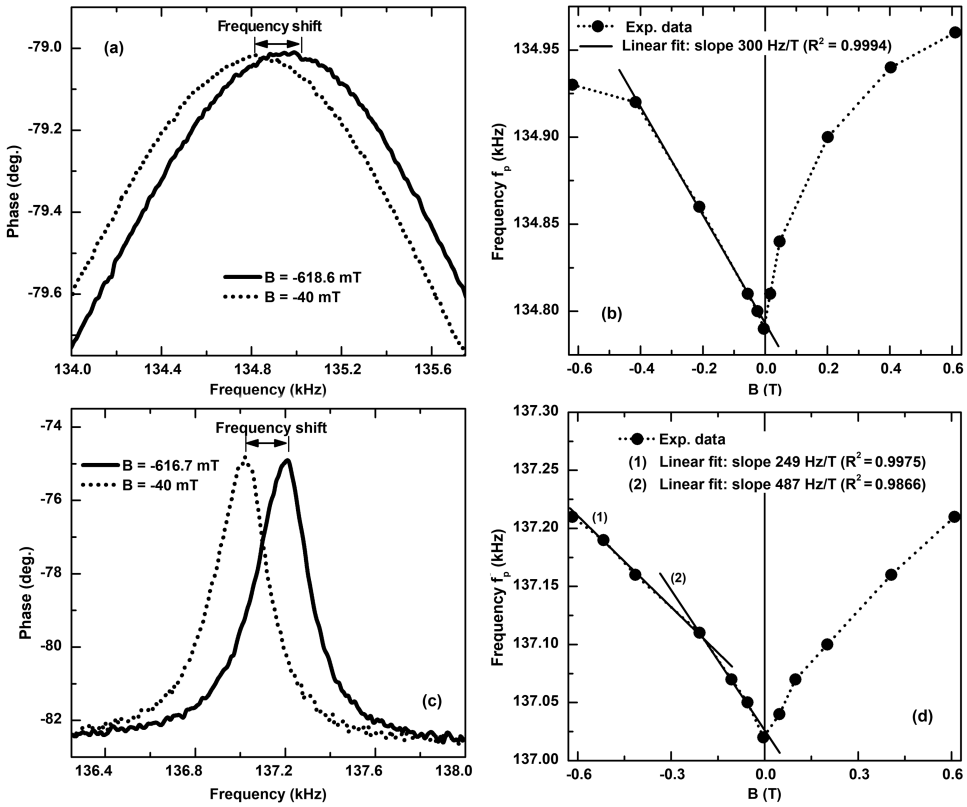

FIG. 7. (a) The impedance phase plotted as a function of frequency at two different values of the out-of-plane DC magnetic field at atmospheric pressure. (b) The resonant frequency f_p extracted from the maximum value of the impedance phase peak and plotted as a function of the out-of-plane DC magnetic field at atmospheric pressure. (c) The impedance phase plotted as a function of frequency at two different values of the out-of-plane DC magnetic field in a 0.5 mbar vacuum environment. (d) The resonant frequency f_p extracted from the maximum value of the impedance phase peak and plotted as a function of the out-of-plane DC magnetic field in a 0.5 mbar vacuum environment.

to the reduction of energy dissipation due to air damping. The resonance frequency values extracted from the impedance phase peak as a function of the out-of-plane DC magnetic field exhibit sensitivities of around 487 Hz/T at a low field (<0.2 T) and 249 Hz/T at a high field (>0.2 T). The asymmetric V-shape shown in Figs. 7(b) and 7(d) with respect to the axis B = 0 could be explained due to the asymmetric strain-magnetic field response of the Tb–Fe–Co layer. These sensitivity values are lower than 5000 Hz/T in a bias magnetic field of 0.2 T reported by Bennett *et al.*[13] on AlN (750 nm)–FeCo (200 nm) double clamped cantilevers. This can be explained due to around 5 times thinner thickness of functional materials in our device leading to a lower response. In addition, the bent shape of single clamped cantilever structures reduces the effective magnetic field on the magnetostrictive layer in a direction perpendicular to the film plane compared to the double clamped cantilever. The resolution of such a device in vacuum can be estimated from the impedance analyzer Hioki IM3570, which has a phase resolution of 10^{-7}deg. In the frequency range around the resonant peak, such a minimum phase change that can be detected with this device corresponds to a minimum frequency change of around 1 Hz. The magnetic field resolutions are thus around 2 and 4 mT for sensitivity values of 487 and 249 Hz/T, respectively. While the sensor design has to be further optimized to improve the performances, it is promising as a micro-magnetoelectric-sensor for magnetic field sensing.

In summary, we demonstrated that resonators based on multiferroic PZT/Tb–Fe–Co thin film multilayers can successfully be used to detect the DC magnetic field by using frequency shift data, with a sensitivity of 487 Hz/T at a low field (<0.2 T) and 249 Hz/T at a high field (>0.2 T). The advantage of such kinds of resonators is the simpler configuration in comparison with the conventional magnetoelectric sensors, thanks to the use of an AC electric field instead of a magnetic field to drive the resonance. This technique allows valuable applications in the fabrication of MEMS devices for magnetic field sensing.

AUTHORS' CONTRIBUTIONS

All authors contributed equally to this work.

ACKNOWLEDGMENTS

This work was partly supported by the French RENATECH network.

DATA AVAILABILITY

The data that support the findings of this study are available from the corresponding author upon reasonable request.

REFERENCES

[1] J. Zhai, Z. Xing, S. Dong, J. Li, and D. Viehland, Appl. Phys. Lett. **88**, 062510 (2006).
[2] M. Li, Y. Wang, J. Gao, J. Li, and D. Viehland, Appl. Phys. Lett. **101**, 022908 (2012).
[3] D. T. H. Giang, P. A. Duc, N. T. Ngoc, and N. H. Duc, Sens. Actuators, A **179**, 78 (2012).
[4] E. Lage, C. Kirchhof, V. Hrkac, L. Kienle, R. Jahns, R. Knöchel, E. Quandt, and D. Meyners, Nat. Mater. **11**, 523 (2012).
[5] S. Marauska, R. Jahns, H. Greve, E. Quandt, R. Knöchel, and B. Wagner, J. Micromech. Microeng. **22**, 065024 (2012).
[6] J. Kiser, P. Finkel, J. Gao, C. Dolabdjian, J. Li, and D. Viehland, Appl. Phys. Lett. **102**, 042909 (2013).
[7] M. Li, D. Berry, J. Das, D. Gray, J. Li, and D. Viehland, J. Am. Ceram. Soc. **94**, 3738 (2011).
[8] S. Dong, J.-F. Li, and D. Viehland, Appl. Phys. Lett. **83**, 2265 (2003).
[9] M. D. Nguyen, M. Dekkers, E. P. Houwman, H. T. Vu, H. N. Vu, and G. Rijnders, Mater. Lett. **164**, 413 (2016).
[10] A. S. Borowiak, G. Niu, V. Pillard, G. Agnus, P. Lecoeur, D. Albertini, N. Baboux, B. Gautier, and B. Vilquin, Thin Solid Films **520**, 4604 (2012).
[11] R. Sandberg, K. Mølhave, A. Boisen, and W. Svendsen, J. Micromech. Microeng. **15**, 2249 (2005).
[12] X. Li, X. Wu, P. Shi, and Z.-G. Ye, Sensors **16**, 69 (2016).
[13] S. P. Bennett, J. W. Baldwin, M. Staruch, B. R. Matis, J. Lacomb, O. M. J. van't Erve, K. Bussmann, M. Metzler, N. Gottron, W. Zappone, R. Lacomb, and P. Finkel, Appl. Phys. Lett. **111**, 252903 (2017).
[14] V. O. Jimenez, V. Kalappattil, T. Eggers, M. Bonilla, S. Kolekar, P. T. Huy, M. Batzill, and M.-H. Phan, Sci. Rep. **10**, 4789 (2020).
[15] L. Méchin, J.-C. Villégier, G. Rolland, and F. Laugier, Physica C **269**, 124 (1996).
[16] S. J. Wang, C. K. Ong, L. P. You, and S. Y. Xu, Semicond. Sci. Technol. **15**, 836 (2000).
[17] R. G. Polcawich, J. S. Pulskamp, D. Judy, P. Ranade, S. Trolier-McKinstry, and M. Dubey, IEEE Trans. Microwave Theory Technol. **55**, 2642 (2007).
[18] N. H. Duc, J. Magn. Magn. Mater. **242-245**, 1411 (2002).
[19] N. H. Duc, K. Mackay, J. Betz, and D. Givord, J. Appl. Phys. **79**, 973 (1996).
[20] M. D. Nguyen, H. Nazeer, K. Karakaya, S. V. Pham, R. Steenwelle, M. Dekkers, L. Abelmann, D. H. A. Blank, and G. Rijnders, J. Micromech. Microeng. **20**, 085022 (2010).
[21] M. D. Nguyen, E. P. Houwman, H. Yuan, B. J. Wylie-Van Eerd, M. Dekkers, G. Koster, J. E. Ten Elshof, and G. Rijnders, ACS Appl. Mater. Interfaces **9**, 35947 (2017).
[22] D. Ambika, V. Kumar, H. Imai, and I. Kanno, Appl. Phys. Lett. **96**, 031909 (2010).
[23] M. S. Weinberg, J. Microelectromech. Syst. **8**, 529 (1999).
[24] M. Dekkers, H. Boschker, M. van Zalk, M. Nguyen, H. Nazeer, E. Houwman, and G. Rijnders, J. Micromech. Microeng. **23**, 025008 (2013).
[25] T. Haccart, E. Cattan, and D. Remiens, Semicond. Phys., Quantum Electron. Optoelectron. **5**, 78 (2002).
[26] N. Banerjee, E. P. Houwman, G. Koster, and G. Rijnders, APL Mater. **2**, 096103 (2014).
[27] E. Hristoforou and A. Ktena, J. Magn. Magn. Mater. **316**, 372 (2007).
[28] T. M. Danh, N. H. Duc, H. N. Thanh, and J. Teillet, J. Appl. Phys. **87**, 7208 (2000).